

Aeolian transport layer

Murilo P. Almeida, José S. Andrade Jr., and Hans J. Herrmann*

*Departamento de Física, Universidade Federal do Ceará,
60455-900 Fortaleza, Ceará, Brazil*

(Dated: June 27, 2018)

We investigate the airborne transport of particles on a granular surface by the saltation mechanism through numerical simulation of particle motion coupled with turbulent flow. We determine the saturated flux q_s and show that its behavior is consistent with a classical empirical relation obtained from wind tunnel measurements. Our results also allow to propose a new relation valid for small fluxes, namely, $q_s = a(u_* - u_t)^\alpha$, where u_* and u_t are the shear and threshold velocities of the wind, respectively, and the scaling exponent is $\alpha \approx 2$. We obtain an expression for the velocity profile of the wind distorted by the particle motion and present a dynamical scaling relation. We also find a novel expression for the dependence of the height of the saltation layer as function of the wind velocity.

PACS numbers: 45.70.Mg, 47.55.Kf, 47.27.-i, 83.80.Hj

The transport of sand by wind is among others responsible for sand encroachment, dune motion and the formation of coastal and desert landscapes. The dominating transport mechanism is saltation as first described by Bagnold [1] which consists of grains being ejected upwards, accelerated by the wind and finally impacting onto the ground producing a splash of new ejected particles. Reviews are given in Refs. [2, 3]. Quantitatively this process is however far from being understood.

Due to Newton's second law the wind loses more momentum with increasing number of airborne particles until a saturation is reached. The maximum number of grains a wind of given strength can carry through a unit area per unit time defines the saturated flux of sand q_s . This quantity has been measured by many authors in wind tunnel experiments and on the field, and numerous empirical expressions for its dependence on the strength of the wind have been proposed [4, 5, 6, 7]. In previous studies theoretical forms have also been derived using approximations for the drag in turbulent flow [8, 9]. All these relations are expressed as polynomials in the wind shear velocity u_* which are of third order, under the assumption that the grain hopping length scales with u_* [1, 4, 8, 9, 10] and otherwise can be more complex [5]. The velocity profile in a particle laden layer has also been the object of measurement [11, 12] and modellization [13]. Surprisingly however very few measurements of the height of the saltation layers as function of u_* have been reported [14] and no systematic data close to the threshold are available. The complete analytical treatment of this problem remains out of reach not only because of the turbulent character of the wind, but also due to the underlying moving boundary conditions in the equations of motion. Despite much research in the past [15] there remain many uncertainties about the trajectory

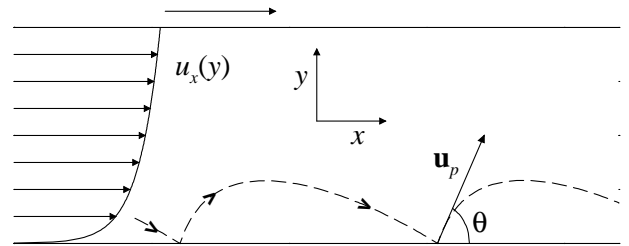


FIG. 1: Schematic representation of the setup showing the mobile wall at the top, the velocity field at different positions in the y -direction and the trajectory of a particle stream (dashed line). At the collision between this stream and the static wall at the bottom, we consider that the particles rebound to the air flow at an ejection angle θ , with only a fraction r of their original kinetic impact energy.

ries of the particles and their feedback with the velocity field of the wind. It is this challenge which motivates the present work.

We will present the first numerical study of saltation which solves the turbulent wind field and its feedback with the dragged particles. As compared to real data, our values have no experimental fluctuations neither in the wind field nor in the particle sizes. As a consequence, we can determine all quantities with higher precision than ever before, and therefore with a better resolution close to the critical velocity at which the saltation process starts.

In order to get quantitative understanding of the layer of airborne particle transport above a granular surface, we simulate the situation inside a two-dimensional channel with a mobile top wall as schematically shown in Fig. 1. We impose a pressure gradient between the left and the right side. Gravity points down, i.e., in negative y -direction. The y -dependence of the pressure drop is adjusted in such a way as to insure a logarithmic velocity profile along the entire channel in the case without particles, as it is expected in fully developed turbulence [16].

*Also at Institute for Computer Physics,
University of Stuttgart
email: hans@ica1.uni-stuttgart.de

More precisely, this profile follows the classical form

$$u_x(y) = (u_*/\kappa)\ln(y/y_0) , \quad (1)$$

where u_x is the component of the wind velocity in the x -direction, u_* is the shear velocity, $\kappa = 0.4$ is the von Karman constant and y_0 is the roughness length which is typically between 10^{-4} and $10^{-2}m$. The upper wall of the channel is moved with a velocity equal to the velocity of the wind at that height in order to insure a non-slip boundary condition.

The fluid mechanics inside the channel is based on the assumptions that we have an incompressible and Newtonian fluid flowing under steady-state and homogeneous turbulent conditions. The fluid is air with viscosity $\mu = 1.7894 \times 10^{-5} kg m^{-1} s^{-1}$ and density $\rho = 1.225 kg m^{-3}$. The Reynolds-averaged Navier-Stokes equations with the standard $k - \epsilon$ model are used to describe turbulence. The numerical solution for the velocity and pressure fields is obtained through discretization by means of the control volume finite-difference technique [17, 18]. The integral version of the governing equations is considered at each cell of the numerical grid to generate a set of non-linear algebraic equations which are pseudo-linearized and solved. The criteria for convergence used in the simulations are defined in terms of residuals, i.e., a measure of the degree to which the conservation equations are satisfied throughout the flow field. In our simulations convergence is achieved only when each of the normalized residuals falls below 10^{-6} .

After having produced a steady-state turbulent flow, we proceed with the simulation of the particle transport along the channel. Assuming that drag and gravity are the only relevant forces acting on the particles, their trajectory can be obtained by integrating the following equation of motion:

$$\frac{d\mathbf{u}_p}{dt} = F_D(\mathbf{u} - \mathbf{u}_p) + \mathbf{g}(\rho_p - \rho)/\rho_p , \quad (2)$$

where u_p is the particle velocity, \mathbf{g} is gravity and $\rho_p = 2650 kg m^{-3}$ is a typical value for the density of sand particles. The term $F_D(\mathbf{u} - \mathbf{u}_p)$ represents the drag force per unit particle mass where

$$F_D = \frac{18\mu}{\rho_p d_p^2} \frac{C_D Re}{24} , \quad (3)$$

$d_p = 2.5 \times 10^{-4} m$ is a typical particle diameter, $Re \equiv \rho d_p |\mathbf{u}_p - \mathbf{u}|/\mu$ is the particle Reynolds number, and the drag coefficient C_D is taken from empirical relations [19]. Each particle in our calculation represents in fact a stream of real grains. It is necessary to take into account the feedback on the local fluid velocity due to the momentum transfer to and from the particles. Specifically, this coupling effect is considered here by alternately solving the discrete and continuous phase equations until the solutions in both phases agree. The momentum transfer from one phase to another is computed by adding the

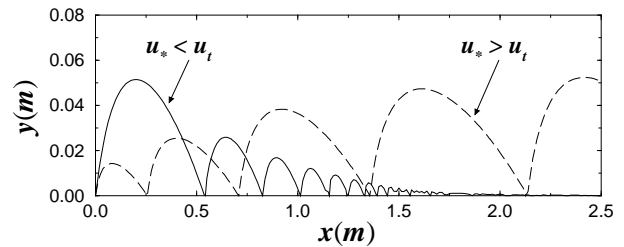


FIG. 2: Typical trajectories of particles computed for $u_* < u_t$ (full line) and $u_* > u_t$ (dashed line).

momentum change of every particle as it passes through a control volume [18],

$$\mathbf{F} = \sum_{\text{particles}} F_D(\mathbf{u} - \mathbf{u}_p)\dot{m}_p\Delta t \quad (4)$$

where \dot{m}_p is the mass flow rate of the particles and Δt the time step. The exchange term Eq. (4) appears as a sink in the continuous phase momentum balance.

In Fig. 1 we see the trajectory of one particle stream and the velocity vectors along the y -direction. Each time a particle hits the ground it loses a fraction r of its energy and a new stream of particles is ejected at that position with an angle θ . The parameters $r = 0.84$ and $\theta = 36^\circ$ are chosen from experimental measurements [20, 21]. We also studied other values for r and θ and even considered a continuous distribution of ejection angles. As expected, the choice of unrealistic values produces unphysical results. More details will be given in Ref. [22].

If u_* is below a threshold value u_t the energy loss at each impact prevails over the energy gain during the acceleration through drag and particle transport comes to a halt as illustrated in Fig. 2. Only for $u_* > u_t$ steady sand motion is achieved. The resulting flux is given by

$$q = m_p n_p \langle u_p \rangle \quad (5)$$

where m_p and $\langle u_p \rangle$ are the mass and the average velocity of the particles, respectively, and n_p is the number of particle streams released. The first added particle streams are strongly accelerated in the channel and their jumping amplitude increases after each ejection until a maximum is reached as seen in Fig. 2. The more particles are injected the smaller is this final amplitude. Beyond a certain number n_s of particle streams, the trajectories however start to lose energy and the overall flux is reduced. This critical value n_s characterizes the saturated flux q_s through Eq. (5).

In Fig. 3 we see the plot of q_s as function of the wind velocity u_* . Clearly, there exists a critical wind velocity threshold u_t below which no sand transport occurs at all. This agrees well with experimental observations [4, 23]. Also shown in Fig. 3 is the best fit to the simulation data using the classical expression proposed by Lettau and Lettau [4],

$$q_s = C_L \frac{\rho}{g} u_*^2 (u_* - u_t) , \quad (6)$$

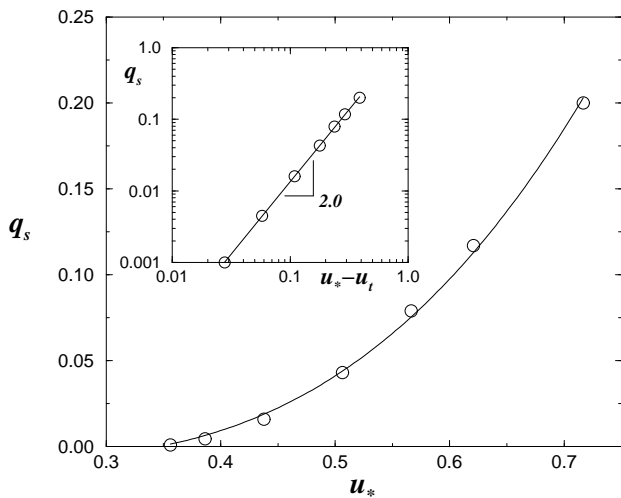


FIG. 3: Saturated flux q_s as function of u_* . The full line is the fit using the expression proposed by Lettau and Lettau [4], $q_s \propto u_*^2(u_* - u_t)$, with $u_t = 0.35 \pm 0.02$. The inset shows the same data in a double logarithmic plot. The straight line corresponds to the least-squares fit to the data of the power-law relation, $q_s \propto (u_* - u_t)^\alpha$, with the exponent $\alpha = 2.01 \pm 0.01$ and the critical point given by $u_t = 0.33 \pm 0.01$.

where C_L is an adjustable parameter. We find very good agreement using fit parameters of the same order as those of the original work and a threshold value of $u_t = 0.35 \pm 0.02$. This is in fact, to our knowledge, the first time a numerical calculation is able to quantitatively reproduce this empirical expression and it confirms the validity of our simulation procedure. Other empirical relations from the literature [8, 9, 10] can also be used to fit these results [22]. Close to the critical velocity u_t interestingly we find that a parabolic expression of the form

$$q_s = a(u_* - u_t)^2 \quad (7)$$

fits the data at least as well as Eq. (6), as can be seen in the inset of Fig. 3. The threshold obtained in this case, namely, $u_t = 0.33 \pm 0.01$, is slightly lower than the one obtained for the classical cubic expression Eq. (6). We believe that our parabolic expression describes correctly the critical behavior very close the transition right above u_t , since at this point the classical assumption of proportionality between the saltation jump length and u_* cannot hold.

Experimentally much more difficult to access is the velocity profile of the wind within the layer of grain transport. This profile clearly deviates from the undisturbed logarithmic form of Eq. (1) because of the momentum the fluid must locally exchange with the particles. In Fig. 4 we show the loss of velocity with respect to the logarithmic profile without particles of Eq. (1) for different values of q as function of the height y . As clearly seen in Fig. 4, the loss of velocity is maximal at the same height y_{max} , regardless of the value of flux q . Except for large values of the flux, dividing the velocity axis by q

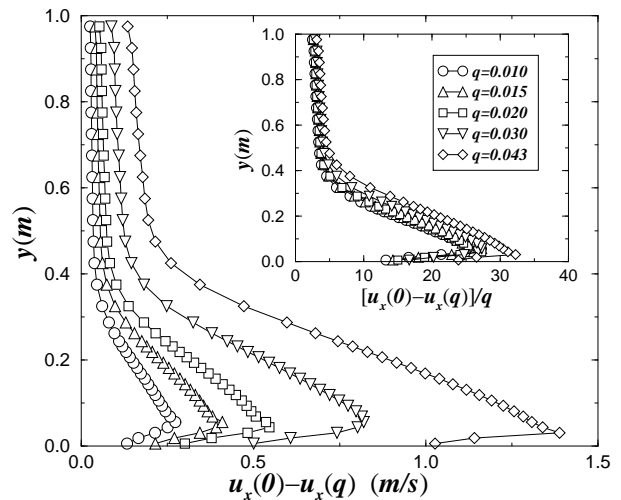


FIG. 4: Profile of the velocity difference $u_x(0) - u_x(q)$ for different values of the flux q at $u_* = 0.51$. The inset shows the data collapse of these data obtained by rescaling the velocity difference with the corresponding q .

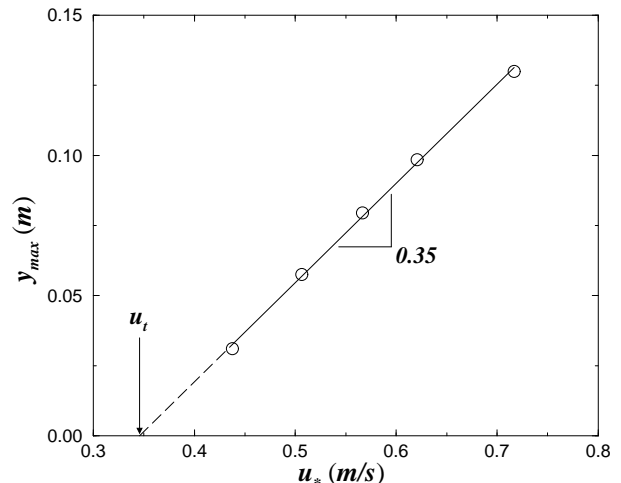


FIG. 5: Height y_{max} of the maximum loss of velocity as function of u_* . The height y_s of the largest probability to find a particle coincides with y_{max} . The solid line corresponds to the best linear fit to the data with a slope equal to 0.35. By extrapolation, the intercept with the x -axis provides an alternative estimate for the critical point, $u_t = 0.35$ m/s, that is consistent with the other calculations.

one can collapse all the profiles quite well on top of each other as can be verified in the inset of Fig. 4.

The position y_{max} of the height of maximum loss depends essentially linearly on u_* as shown in Fig. 5. This is consistent with the observation that the saltation jump length is proportional to u_* [9]. The proportionality constant obtained from the best linear fit to the data is 0.35 s. Quantitatively the data in Fig. 5 also fit very well into the experiment data plots of Ref. [14]. By extrapolation to $y_{max} = 0$, we obtain an alternative estimate for

the threshold velocity, $u_t = 0.35 \text{ m/s}$, that is consistent with the values calculated before from the fits to the data using Eqs. (6) and (7).

Whoever has been in the desert or on a beach during a very windy day knows that the saltation process in nature looks like a sheet of particles floating above ground at a certain height y_s which strongly depends on the wind velocity. This height corresponds to the position of the largest likelihood to find a particle as obtained from the maximum of the density profile of particles as function of height y . Fig. 5 implies that the profile of velocity difference of the wind has a minimum at a similar height, which is consistent with the maximal loss of momentum. Within the error bars our results in fact yield that y_s coincides with the values of y_{max} in Fig. 5. More details will be presented in Ref. [22]. It is important to note that both heights, y_{max} and y_s , also have the same linear dependence on u_* .

We have shown in this letter results of simulations giving insight about the layer of granular transport under conditions of turbulent flow. The lack of experimental

noise allows for a precise study close to the critical threshold velocity u_t that lead us to a parabolic dependence of the saturated flux. In addition, we show that the velocity profile disturbed by the presence of grains scales linearly with the flux of grains, except close to saturation. Notably a characteristic height appears at which the momentum loss in the fluid and the grain density are maximized. Moreover, this height increases linearly with the wind velocity u_* . It would be very interesting to verify experimentally these novel predictions. The present model can be extended in many ways including the study of the dependence of the aeolian transport layer on the grain diameter, the gas viscosity, and the solid or fluid densities. This would allow to calculate, for instance, the granular transport on Mars and compare with the expression presented in Ref. [10]. Work in this direction is under way [22].

We thank Keld Rasmussen, Eric Parteli, Josué Mendes Filho and Ascânio Dias Araújo for discussions and CNPq, CAPES, FUNCAP and the Max-Planck prize for financial support.

-
- [1] R. A. Bagnold, *The Physics of blown sand and desert dunes* (Methuen, London, 1941).
 - [2] R. S. Anderson, M. Sørensen and B. B. Willetts, *Acta Mech. (Suppl.)* **1**, 1 (1991).
 - [3] H. J. Herrmann, in *The Physics of Granular Media*, eds. H. Hinrichsen and D. Wolf (Wiley VCH, Weinheim, 2004), p. 233-252.
 - [4] K. Lettau and H. Lettau, in *Exploring the world's driest climate*, eds. H. Lettau and K. Lettau, Center for Climatic Research (Univ. of Wisconsin, Madison, 1978).
 - [5] B. T. Werner, *J. Geol.* **98**, 1 (1990).
 - [6] K. R. Rasmussen and H. E. Mikkelsen, *Acta Mechanica Suppl.* **1**, **135** (1991).
 - [7] Y.-H. Zhou, X. Guo and X. J. Zheng, *Phys. Rev. E* **66**, 021305 (2002).
 - [8] P. R. Owen, *J. Fluid Mech.* **20**, 225 (1964).
 - [9] M. Sørensen, in *Proc. Int. Wkshp. Physics of Blown Sand*, Vol.1 (Univ. of Aarhus, Denmark, 1985), p. 141; *Acta Mech. (Suppl.)* **1**, 67 (1991).
 - [10] B. R. White, *Geophys. Res.* **84**, 4643 (1979).
 - [11] G. R. Butterfield, in *Turbulence: Perspectives on Flow and Sediment Transport*, eds. N. J. Clifford, J. R. French and J. Hardisty, Chapter 13 (John Wiley, 1993), p.305.
 - [12] K. Nishimura and J. C. R. Hunt, *J. Fluid. Mech.* **417**, 77 (2000).
 - [13] J. E. Ungar and P. K. Haff, *Sedimentology* **34**, 289 (1987).
 - [14] Z. Dong, X. Liu, H. Wang, A. Zhao and X. Wang, *Geomorphology* **49**, 219 (2002).
 - [15] P. Nalpanis, J. C. R. Hunt and C. F. Barrett, *J. Fluid Mech.* **251**, 661-685 (1993).
 - [16] L. Prandtl, in *Aerodynamic Theory*, ed. W. F. Durand, Vol. III (Springer, Berlin, 1935), p.34.
 - [17] S. V. Patankar, *Numerical Heat Transfer and Fluid Flow* (Hemisphere, Washington DC, 1980)
 - [18] The FLUENT (trademark of FLUENT Inc.) commercial package for fluid dynamics analysis is used in this study.
 - [19] S. A. Morsi and A. J. Alexander, *J. Fluid Mech.* **55**, 193 (1972).
 - [20] R. S. Anderson and P. K. Haff, *Science* **241**, 820 (1988).
 - [21] F. Rioual, A. Valance and D. Bideau, *Phys. Rev. E* **62**, 2450-2459 (2000).
 - [22] M. P. Almeida, J. S. Andrade Jr. and H. J. Herrmann, preprint in preparation.
 - [23] R. A. Bagnold, *Proc. R. Soc. Lond A* **167**, 282 (1938).